Ohmic potential drop and gas bubble radius distribution in alkaline water electrolysis

Ohmic potential drop and gas bubble radius distribution in alkaline water electrolysis.

Dr. B.E. Bongenaar-Schlenter, Prof. E. Barendrecht, Dr. L.J.J. Janssen and Dr. S.J.D. van Stralen
Eindhoven University of Technology
P.O. Box 513, 5600 MB Eindhoven, The Netherlands.

SUMMARY

Energy losses in water electrolysis are caused by the evolution of gas bubbles. The main aim of this investigation is to obtain a dimensionless correlation for the ohmic resistance between working electrode and diaphragm in the presence of gas bubbles. The resistance has been determined in dependence of KOH-concentration, temperature, pressure, gas to liquid volumetric ratio at the outlet of the cell, nature of nickel electrode surface and distance between working electrode and diaphragm. The reduced ohmic resistance is given by a dimensionless correlation.

The effects of various parameters on the average bubble radius and bubble radius distribution at the outlet of the cell have been studied. From the experimental results also a dimensionless correlation has been deduced for the reduced average bubble radius.

KURZFASSUNG

Die Entwicklung von Gasblasen verursacht erhebliche Energieverluste bei der Wasserelektrolyse. Die Hauptaufgabe unserer Untersuchung ist die Formulierung einer dimensionslosen mathematischen Beziehung für den Ohmschen Widerstand zwischen Arbeitselektrode und Diaphragma und für den durchschnittlichen Blasenradius.

Der Widerstand wird in Abhängigkeit von KOH-Konzentration, Temperatur, Druck, Verhältnis zwischen Gasblasenvolumen

und Flüssigkeitsvolumen am Austritt aus der Elektrolysezelle, Art der Nickelelektrodenoberfläche und Abstand zwischen Arbeitselektrode und Diaphragma bestimmt. Der reduzierte Ohmsche Widerstand wird in einer dimensionslosen Beziehung dargestellt.

Der Einfluß der verschiedenen Parameter auf den durchschnittlichen Blasenradius und auf die Verteilung des Blasenradius's am Austritt aus der Elektrolysezelle sind untersucht worden.
Für den reduzierten durchschnittlichen Blasenradius wird eine dimensionslose Beziehung abgeleitet.

RESUME

Des pertes d'énergie pendant l'électrolyse d'eau proviennent d'une libération de bulles gazeuses. Le but des recherches décrites ci-dessous est d'obtenir une relation adimensionelle pour la résistance ohmique entre l'électrode de production et le diaphragme, en présence des bulles de gaz. Cette résistance a été régistrée en dépendance de la concentration en KOH, de la température, de la preasion, de la proportion du volume de gaz au volume de liquide, sortants de la cellule; de la caractéristique de la surface de l'électrode en nickel et de la distance entre l'électrode et le diaphragme.

La résistance ohmique réauite est donnée par une corrélation sans dimensions. L'influence des paramètres différents sur le rayon de bulle moyen et sur la distribution à la sortie de la cellule a été étudiée. Ainsi résulte de nos experimentations une relation adimensionelle pour le diamètre des bulles réduit en moyenne.

1. INTRODUCTION.

The energy efficiency of the alkaline water electrolysis process is reduced by the increase in ohmic potential drop in the electrolysis cell, due to the presence of hydrogen and oxygen bubbles on the electrodes and dispersed in the electrolyte between anode and cathode.
This increase in ohmic potential drop is affected by a number of parameters such as geometry of the cell, current density, solution flow velocity, temperature, pressure and the nature of the electrodes, the diaphragm, the electrolyte and the gas evolved.
The effects of current density, flow velocity of the electrolyte, electrode and diaphragm on the ohmic potential drop between working electrode and diaphragm have been studied by Janssen et al. /1/, using a vertical

rectangular cell with vertical electrodes 50 cm in height.
A dimensionless correlation between the increase in ohmic resistance due to the presence of bubbles and these parameters has been proposed. In the present investigation additionally the effects of KOH-concentration, temperature, pressure, gas to liquid volumetric ratio at the outlet of the cell and nature of the nickel electrode surface on the ohmic resistance of the cell and on the average bubble radius and bubble radius distribution at the outlet of the cell have been studied.

2. EXPERIMENTAL SET-UP.

The experiments have been carried out in two electrolysis cells. One cell, suitable for measurements at atmospheric pressure, consists of a transparent acrylate compartment for the counter electrode and a non-transparent acrylate compartment for the working electrode.
The second electrolysis cell for potential drop measurements, suitable at pressures up to 10 bar, is essentially the same as the one used at atmospheric pressure, except that it is made of stainless steel. To be able to study the gas bubbles in the electrolysis cell at various heights, the cell contains five glass windows.
Further details on the experimental set-ups are given in previous papers /1, 2, 3/.

3. RESULTS.

3.1. Ohmic potential drop.

3.1.1. Effect of the gas to liquid volumetric ratio at the outlet of the electrolysis cell.

The gas to liquid volumetric ratio at the outlet of the cell can be varied by changing either the current density or the solution flow velocity in the cell.

The gas/liquid volumetric ratio is usually expressed in terms of a gas void fraction. A gas/liquid volumetric ratio of 1 corresponds with a gas void fraction of 0.5.
In Fig. 1 the ohmic potential drop, ΔV, is plotted as a function of the current density, i, for various solution flow velocities, v_l. Only the results for capillary 1 are shown in this figure, since similar results were found for the other capillaries and for the ohmic potential drop between anode and cathode.
The figure shows that ΔV is proportional to the current density. Consequently, the resistance, $R = \Delta V/i$, between the capillary and the working electrode is independent of the current density in the current

density range studied. This result has been found for both hydrogen and oxygen evolving electrodes.

From the same figure it follows that the ohmic resistance decreases at increasing solution flow velocity. It has been found that the log R vs log v_g curves are straight and the slopes depend on the nature of the electrode material. They are, however, almost independent of distance between electrode and diaphragm, temperature, pressure and height in the cell.

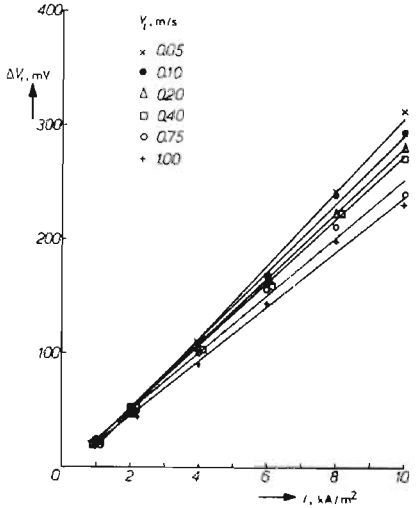

Fig. 1 ΔV_l as a function of current density for a hydrogen evolving nickel electrode at [KOH] = 30 wt%, T = 353 K, d_{wm} = 3 mm and various solution flow velocities.

They vary between approximately -0.05 for an oxygen evolving teflon bonded nickel cobalt oxide electrode and -0.15 for a hydrogen evolving Raney type nickelsulfide electrode.

Since the resistance does depend on the solution flow velocity but does not depend on the current density, the average gas void fraction cannot be used to describe the resistance between working electrode and diaphragm.

3.1.2. Effect of nature of the electrode surface.

The effect of the nature of the cathode has been studied on three different kinds of electrodes, viz. a nickel electrode, a nickel-teflon electrode and a Raney type nickelsulfide electrode. Fig. 2 shows the ohmic potential drops between capillary and the respective working electrodes, as a function of current density. The ohmic potential drop is largest for the nickel-teflon

electrode. At relatively high solution flow velocities, the ohmic potential drop for a nickelsulfide electrode is slightly lower than for a bare nickel electrode cf. Fig. 1.

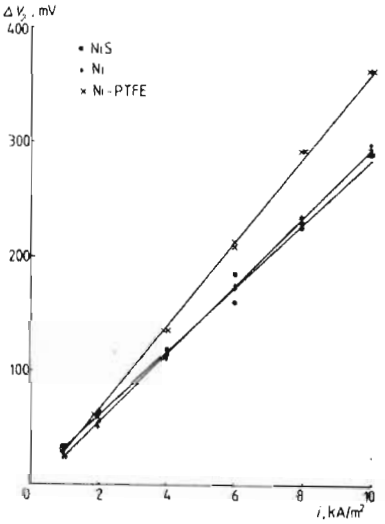

Fig. 2
The ohmic potential drop as a function of current density for a nickel, a nickel-sulfide and a nickel-teflon cathode at [KOH] = 30 wt%, T = 353 K, d_{wm} = 3 mm and v_{ℓ} = 0.5 m/s.

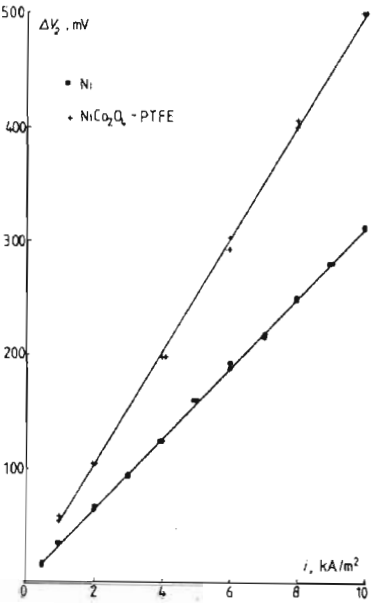

Fig. 3
The ohmic potential drop as a function of current density for a nickel and a teflon bonded nickel cobalt oxide anode at [KOH] = 30 wt%, T = 353 K, d_{wm} = 3 mm and v_{ℓ} = 0.5 m/s.

The activation overpotential for this electrode, however, is significantly lower than for the nickel electrode.

Nickel and teflon bonded nickel cobalt oxide have been used as anode materials. Fig. 3 shows the results obtained for these electrodes. The ohmic potential drop for an oxygen evolving teflon bonded nickel cobalt oxide electrode exceeds the corresponding value for a nickel anode. No significant differences in activation overpotential between these electrodes have been found.

The large ohmic resistance for teflon containing electrodes is probably due to a different bubble behavlour on these electrodes. Because of the poor

wettability of the teflon, relatively large bubbles are formed which remain on the electrode for a longer period than in the case of a nickel electrode.

3.1.3. Effect of temperature.

The ohmic potential drop between working electrode and diaphragm decreases at increasing temperature. The reduced resistance, R/R_p, is calculated from the potential drop measurements in combination with the experimental R_p values given in /4/. It has been found that the reduced resistance is practically independent of temperature in the range 333-353 K.

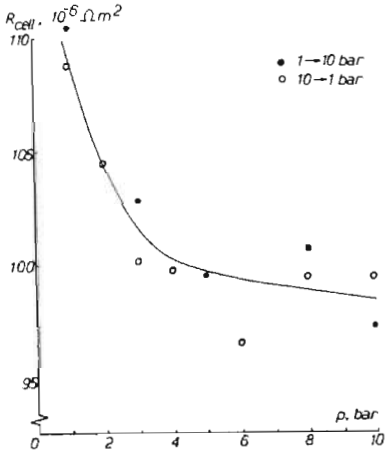

Fig. 4 The ohmic resistance between anode and cathode as a function of pressure. T = 353 K, d_{wm} = 3 mm, v_g = 0.5 m/s and [KOH] = 30 wt%.

3.1.4. Effect of KOH-concentration.

The effect of KOH-concentration has only been determined for a hydrogen evolving nickel working electrode. The reduced resistance between a capillary and the working electrode and between anode and cathode were measured as a function of the electrolyte concentration for two solution flow velocities. Although the ohmic resistance decreases at increasing KOH-concentration up to a value of approximately 30 wt%, the reduced resistance showed a maximum at approximately 16 wt% KOH, because of the ohmic resistance decrease of the pure electrolyte with increasing KOH-concentration.

3.1.5. Effect of pressure.

At elevated pressures up to 10 bar, the ohmic potential remains proportional to the current density. In Fig. 4 the ohmic resistance is plotted in dependence on pressure for a hydrogen evolving nickel electrode. From this figure it follows, that the ohmic resistance decreased at increasing pressure. This effect is more pronounced at lower pressures than at higher pressures. A plot of log R versus log p shows a straight line with a slope of approximately -0.03.

This slope is practically independent of solution flow velocity, distance between electrode and diaphragm and height in the electrolysis cell and only slightly dependent on the nature of the electrode surface.

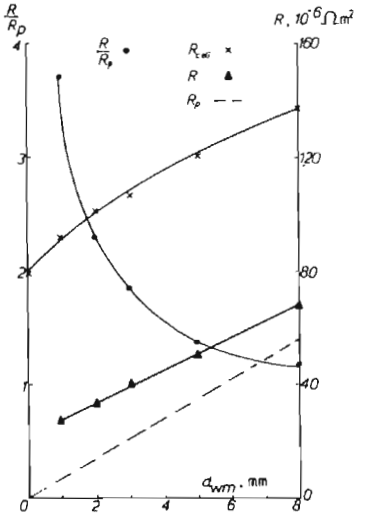

Fig. 5 The resistance and the reduced resistance between cathode and diaphragm and the resistance between anode and cathode as a function of distance between cathode and diaphragm.
T = 353 K, v_ℓ = 0.5 m/s, [KOH] = 30 wt%.

3.1.6. Effect of distance between working electrode and diaphragm.

The distance between working electrode and diaphragm, d_{wm}, has been varied from 10 mm to 0 mm. Fig. 5 shows the resistance and the reduced resistance as a function of distance for a hydrogen evolving nickel electrode. The ohmic resistance decreases almost linearly, with decreasing distance. The curve has the same slope as the curve for the pure electrolyte. This indicates that the bubbles near the electrode determine the increase in

ohmic potential drop. The reduced resistance, however, increases at decreasing distance.

Experiments showed that the slope of the log R/R_p - log d_{wm} plot depends on both the height in the cell and the nature of the electrode. It is, however, independent of solution flow velocity. The slopes vary from approximately -0.20 to -0.50.

3.1.7. Effect of the geometry of the electrode.

The effect of the geometry of the electrodes has been studied at various solution flow velocities and pressures. Six different electrode geometries have been used, i.e., a plate electrode, a venetian blind electrode, a woven gauze electrode, an expanded metal gauze electrode and two types of Veco gauze electrodes. Detailed information on these electrodes is shown in Fig. 6.

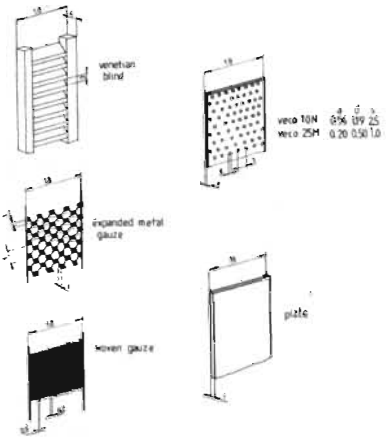

Fig. 6 Different types of working electrodes as used for potential drop measurements. Dimensions are given in mm. The electrodes are 50 cm in length.

To ensure that only the electrode configuration effect and not the effect of the nature of the electrode surface is studied, each electrode is nickel plated in a Watts bath at a current density of 2 A/dm^2 for one hour. During this process a nickel layer of approximately 20 µm is deposited on the electrode surface.

In Figs. 7 and 8 the ohmic potential drop between anode and cathode is shown in dependence on current density for various electrodes in case of gap widths between the working electrode and the diaphragm, d_{wm}, of 3 and 0 mm

and at solution flow velocities, v_ℓ, of 0 and 0.4 m/s. Fig. 7 shows that, at free convection (v_ℓ=0 m/s) and d_{wm} = 3 mm, the ohmic resistance for the expanded metal gauze electrode is smaller than the corresponding values for the other electrodes. The ohmic potential drop measured for various electrodes increases in the sequence expanded metal gauze electrode, woven gauze electrode, Veco gauze 25 M electrode, venetian blind electrode, plate electrode and Veco gauze 10 N electrode.

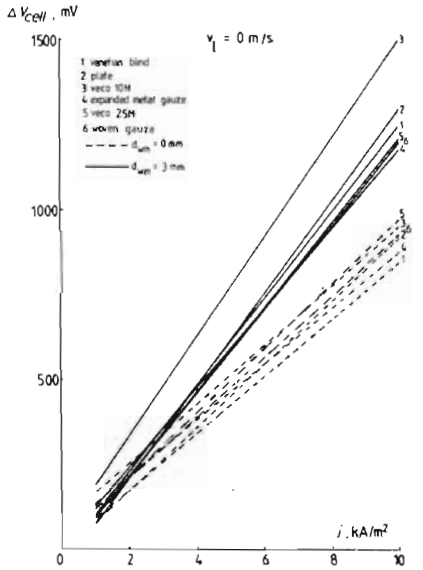

Fig. 7 Ohmic potential drop between anode and cathode as a function of current density for various electrode geometries.
[KOH] = 30 wt%, T = 353 K, v_ℓ = 0 m/s.

At d_{wm} = 0 mm, the venetian blind electrode is more favourable in comparison to the expanded metal gauze electrode. For this configuration the ohmic potential drop for the plate electrode is surprisingly low. Possibly hydrogen gas diffuses through the asbestos diaphragm, where it is carried to the back of the counter electrode together with the evolved oxygen gas. A comparison of these figures shows that, at d_{wm} = 3 mm, the differences between the different electrodes decrease at increasing solution flow velocity. The effect of solution flow velocity on the ohmic potential drop at d_{wm} = 0 mm, is small. Apparently, for all electrodes studied, the ohmic resistances between anode and cathode at d_{wm} = 3 mm exceed those at

d_{wm} = 0 mm.

The effect of pressure on the ohmic resistance in the cell has been found to be independent of electrode geometry. For all electrodes studied the ohmic resistance decrease at increasing pressure. The effects are more pronounced at lower than at higher pressures.

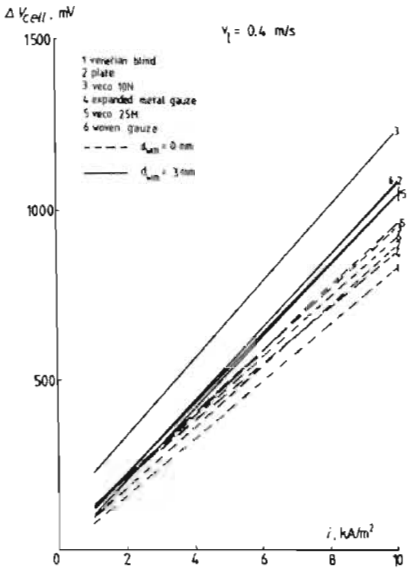

Fig. 8 Ohmic potential drop between anode and cathode as a function of current density for various electrode geometries.
[KOH] = 30 wt%, T = 353 K, v_g = 0.4 m/s.

3.2. Bubble radius.

3.2.1. Introduction.

The average bubble radius and the bubble radius distribution at the outlet of the cell depend on two main factors, i.e. the departure radius of the bubbles from the electrode surface and the coalescence behaviour of the detached bubbles in the electrolyte.

When a parameter of the electrolysis process is varied both the departure radius and the coalescence behaviour, may be affected. Consequently the interpretation of the results is very difficult; especially for oxygen bubbles, because they coalesce more frequently than hydrogen bubbles.

3.2.2. Effect of current density.

In Fig. 9, the average radii, $\bar{R}_b$, for oxygen and hydrogen bubbles evolved on various electrodes are shown in dependence on current density. It has been found that the average radius for hydrogen bubbles evolved on a nickel electrode is independent or only slightly dependent on current density. The average bubble radii for oxygen bubbles generated on a nickel and on a teflon bonded nickel cobalt oxide electrode and for hydrogen bubbles evolved on a nickelsulfide electrode increase at increasing current density.

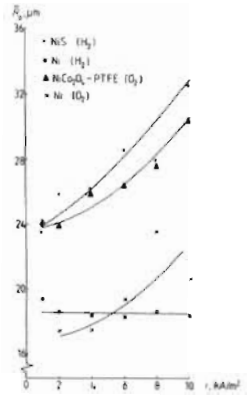

Fig. 9
The average bubble radius for oxygen and hydrogen bubbles evolved on various electrodes as a function of current density.
T = 353 K, v_ℓ = 0.5 m/s,
d_{wm} = 3 mm and [KOH] = 30 wt%

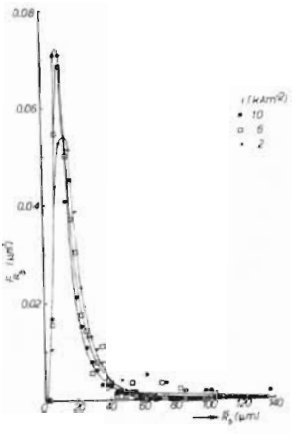

Fig. 10
Bubble radius distribution curves for hydrogen bubbles evolved on a nickel electrode at 2,6 and 10 kA/m^2.

T = 353 K, v_ℓ = 0.5 m/s,
d_{wm} = 3 mm and [KOH] = 30 wt%

Fig. 10 shows the bubble size distribution for a hydrogen evolving nickel electrode for i = 10 kA/m^2, i = 6 kA/m^2 and i = 2 kA/m^2. At high current density there is a sharp peak with a top at 9 µm and the maximal bubble radius is about 150 µm. At lower current densities the peak broadens and its top shifts to 13 µm. The maximal bubble radius decreases to about 80 µm. The small bubbles probably detached from the electrode surface without coalescence while the larger bubbles are due to coalescence of small bubbles.

In Fig. 11 the bubble size distribution curves for an oxygen evolving nickel electrode are shown at i = 10 kA/m^2 and i = 2 kA/m^2. The peak of the curve

becomes lower and broader at high current densities, probably because of the increase in coalescence of the bubbles. The position of the peak does not change markedly.

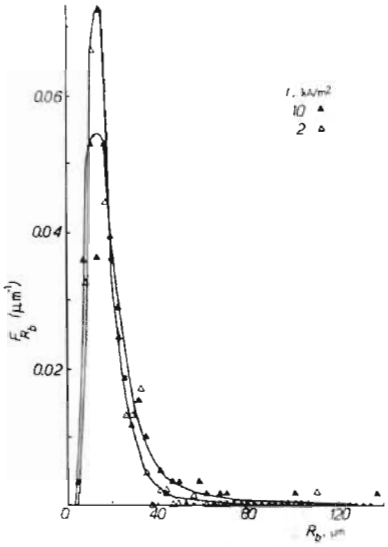

Fig. 11 Bubble radius distribution curves for oxygen bubbles evolved on a nickel electrode at 2 and 10 kA/m^2.
T = 353 K, v_ℓ = 0.5 m/s, d_{wm} = 3 mm and [KOH] = 30 wt%

A plot of $\bar{R}_b$ versus i on a double logarithmic scale shows straight lines with slopes varying from 0 for a hydrogen evolving nickel electrode to 0.16 for an oxygen evolving electrode.

3.2.3. Effect of solution flow velocity.

In Fig. 12 the average bubble radii for oxygen and hydrogen bubbles evolved on various electrodes are shown as functions of solution flow velocity. At increasing solution flow velocity, the average bubble radius for both oxygen and hydrogen bubbles decreases. This effect is most pronounced at low solution flow velocities. Plots of log $\bar{R}_b$ as a function of log v_ℓ show straight lines with slopes varying between -0.06 for both an oxygen evolving teflon bonded nickel cobalt oxide electrode and a hydrogen evolving nickel electrode and -0.40 for an oxygen evolving nickel electrode.

3.2.4. Effect of the nature of the electrode surface.

Bubbles evolved on teflon containing electrodes e.g. teflon bonded nickel cobalt oxide and nickel-teflon electrodes or on an nickelsulfide electrode show a larger average bubble radius than bubbles evolved on nickel electrodes (Fig. 12).

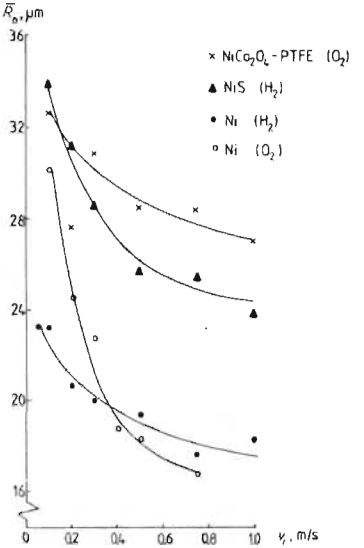

Fig. 12 The average bubble radius for oxygen and hydrogen bubbles evolved on various electrodes as a function of solution flow velocity.
T = 353 K, i = 4 kA/m^2, d_{wm} = 3 mm and [KOH] = 30wt%

3.2.5. Effect of temperature.

The average bubble radius was determined as a function of temperature in the temperature range 30 - 80^{0}C at i = 4 kA/m^2 and v_ℓ = 0.5 m/s for various electrodes. It has been found that the average bubble radius for oxygen as well as for hydrogen bubbles is practically independent of temperature in the investigated range. The bubble size distribution curves are alao independent of temperature.

3.2.6. Effect of KOH-concentration.

The effect of KOH-concentration on the average bubble radius has been investigated using a hydrogen evolving nickel electrode. It has been found that the average radius decreases at increasing KOH-concentration.
A plot of $\bar{R}_b$ in dependence on KOH-concentration on a double logarithmic scale shows a straight line with a slope of -0.22 at a solution flow

velocity of 0.25 m/s and a slope of -0.12 at 0.5 m/s.

3.2.7. Effect of pressure.

The effect of pressure on the average radius of hydrogen bubbles evolved on a nickel electrode was investigated in the pressure range from 1 to 10 bar. It has been found that the average radius decreases at increasing pressure, due to the decrease in the occurrence of coalescence at elevated pressures. The effect is more pronounced at lower solution flow velocities.
Plots of $\bar{R}_b$ versus p on a double logarithmic scale show straight lines with slopes varying from -0.24 at a solution flow velocity of 0.1 m/s to -0.09 at a velocity of 0.5 m/s. The slopes are practically independent of the nature of the gas evolved.

3.2.8. Effect of distance between working electrode and diaphragm.

The distance between working electrode and diaphragm has been varied from 10 to 0 mm. The average radii are found to be independent of distance between the working electrode and the diaphragm.

4. DISCUSSION.

4.1. Ohmic potential drop in the electrolysis cell.

The flow situation and the gas void distribution in the electrolysis cell under practical conditions are very complicated. Although one may argue that the average solution flow velocity in the 3 mm wide area between the electrode and the diaphragm will be subatantially lower than the velocity in the 12 mm wide area at the back of the electrode, the values of the average flow velocities, the flow profiles, the flows through the electrodes and the widths of the bubble layers adjacent to the electrodes are not known. Further it is unknown which part of the evolved gas volume is deviated to the back of the electrodes.
For these reasons it is practically impossible to predict the effect of various electrode geometries in a quantitative way.
From the experiments it follows that generally the venetian blind electrode is the most favourable electrode configuration for the ohmic resistance in the electrolysis cell.
Therefore, a dimensionless correlation is derived from the experimental results obtained in this situation.
It is noted that the current is assumed to be distributed uniformly over the entire electrode surface.
Janssen et al. /1/ have proposed a dimensionless correlation, which describes the reduced ohmic resistance increase due to the presence of bubbles in the solution layer between working electrode and diaphragm, during alkaline water electrolysis. This relation has to be extended to include the effects of

electrolyte concentration, temperature and pressure. To diminish the number of empirical constants, a correlation describing the reduced ohmic resistance, instead of the reduced ohmic resistance increase, is proposed.
It has been found that, within experimental scatter, the reduced resistance is independent of current density (4.3.1.) and of temperature (4.3.3.) in the ranges investigated. Consequently, these parameters do not occur in the dimensionless correlation.
In Table 1, the numerical values of K_1, n_1, n_2, n_3 and n_4 are given for the 4 kinds of electrodes in the present experiments.

nature of electrode	gas evolved	K_1	n_1	n_2	n_3	n_4
Veco gauze	H_2	1.9	-0.08	-0.30	-0.03	0.05
NiS	H_2	2.9	-0.15	-0.40	-0.03	n.d.
Ni-PTFE	H_2	2.1	-0.08	-0.30	-0.03	n.d.
Veco gauze	O_2	1.3	-0.06	-0.35	-0.03	n.d.
$NiCo_2O_4$-PTFE	O_2	1.7	-0.05	-0.45	-0.03	n.d.

Table 1 Numerical values of empirical constants for various electrodes.

To obtain a dimensionless correlation the Reynolds number, Re, the reduced distance between working electrode and diaphragm, D_{wm}, and the reduced pressure, P, are introduced.
The Reynolds number for a flowing liquid is defined by $Re = d_{hyd} \cdot v_\ell / \nu$. The hydraulic diameter, d_{hyd}, equals 4× cross sectional area of the working electrode compartment divided by the circumference of the rectangular compartment and is constant during all experiments. The variations in the kinematic viscosity, ν, of the electrolyte are relatively small in the range studied.
Consequently, within experimental scatter, the Reynolds number can be used to describe the dependence of the reduced resistance on the solution flow velocity.
The reduced distance between working electrode and diaphragm is defined by the distance between working electrode and diaphragm divided by the distance between the backwall of the working electrode compartment and the diaphragm. The latter quantity has been chosen because the bubbles evolved on the electrode can spread over the entire compartment.
The reduced pressure is obtained by relating the pressure to the atmospheric pressure , p_0.

Using the forementioned parameters, the following dimensionless correlation is obtained:

$$R/R_p = K_1 . Re^{n_1} . D_{wm}^{n_2} . P^{n_3} . (|[KOH]/|[KOH]-[KOH]_{max}|)^{n_4}$$ where

K_1, n_1, n_2, n_3 and n_4 are empirical constants.

4.2. Bubble radius.

From the experiments it has been found that the average bubble radius at the outlet of the electrolysis cell is practically independent of temperature and distance between working electrode and diaphragm in the ranges studied. Consequently, these parameters do not appear in the dimensionless correlation.

nature of electrode	gas evolved	K_2 v_ℓ= 0.5 m/s	n_5	n_6	n_7 v_ℓ= 0.25	n_7 v_ℓ= 0.5 m/s	n_8 v_ℓ= 0.25	n_8 v_ℓ= 0.5 m/s
Veco gauze	H_2	5.1×10^{-3}	0	-0.10	-0.20	-0.13	-0.22	-0.12
NiS	H_2	3.6×10^{-3}	0.11	-0.04	n.d.		n.d.	
Ni-PTFE	H_2	4.6×10^{-3}	0	-0.11	n.d.		n.d.	
Veco gauze	O_2	1.8×10^{-2}	0.16	-0.24	0	+0.07	n.d.	
$NiCo_2O_4$-PTFE	O_2	2.1×10^{-3}	0.09	+0.03	n.d.		n.d.	

Table 2 Numerical values of empirical constants for various electrodes.

n.d. = not determined

To obtain a dimensionless correlation the reduced average bubble radius and the gas to liquid volumetric ratio at the outlet of the electrolysis cell, V_g/V_ℓ, the Reynolds number and the reduced pressure are used. The KOH-concentration is already dimensionless because it is expressed in wt%. The reduced average bubble radius at the outlet of the cell is defined by the average bubble radius divided by the distance between the backwall of the working electrode compartment to the diaphragm. The gas to liquid volumetric ratio at the outlet of the cell is proportional to $i/p.v_\ell$. Incorporating the dimensionless parameters in the relation, the following dimensionless correlation results:

$$\bar{R}_b/d_{bm} = K_2 . (V_g/V_\ell)^{n_5} . Re^{n_6} . p^{n_7} . [KOH]^{n_8}$$ where

K_2, n_5, n_6, n_7 and n_8 are empirical constants.

In Table 2 the numerical values of K_2, n_5, n_6, n_7 and n_8, obtained from our experiments, are given for the cases of the 4 kinds of electrodes studied.

LITERATURE

/1/ L.J.J. Janssen, J.J.M. Geraets, E. Barendrecht and S.J.D. van Stralen, Electrochim. Acta 27 (1982), 1207.

/2/ C.W.M.P. Sillen, thesis, Eindhoven 1982.

/3/ B.E. Bongenaar-Schlenter, L.J.M. Konings, C.J. Smeijers, J.H.G. Verbunt, E. Barendrecht, L.J.J. Janssen, W.M. Sluijter and S.J.D. van Stralen in Hydrogen as an Energy Carrier, Proceedings of the 3th International Seminar, held in Lyon, 25-27 May 1983, editioned by G. Imarisio and A.S. Strub, 206.

/4/ B.E. Bongenaar-Schlenter, thesis, Eindhoven 1984.

LIST OF SYMBOLS AND SI-UNITS

d_b	bubble diameter	(m)
d_{bm}	distance between the backwall of the working electrode compartment and the diaphragm	(m)
d_{hyd}	hydraulic diameter of the working electrode compartment	(m)
d_{wm}	distance between the working electrode and the diaphragm resp. the tip of the Luggin capillarry	(m)
D_{wm}	reduced distance between the working electrode and the diaphragm; $D_{wm} = d_{wm}/d_{bm}$	(-)
i	current density	(A/m^2)
K_i	empirical constant	(-)
n_i	empirical constant	(-)
p_o	atmospheric pressure	(N/m^2)
P	reduced pressure; $P = p/p_o$	(-)
R	resistance	(Ω)
R_b	bubble radius	(m)
R_p	resistance of the pure electrolyte	(Ω)
Re	Reynolds number	(-)
T	temperature	(K)
v_l	liquid flow velocity	(m/s)
V_G	volumetric gas production rate	(m^3/s)
V_l	volumetric liquid flow rate	(m^3/s)
ΔV	ohmic potential drop between the working electrode and the Luggin capillary	(V)
ν	kinematic viscosity	(m^2/s)